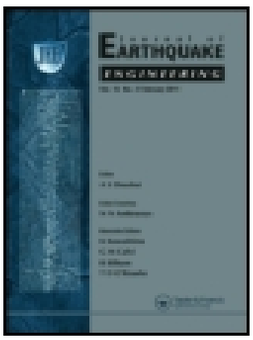

Journal of Earthquake Engineering

ISSN: 1363-2469 (Print) 1559-808X (Online) Journal homepage: http://www.tandfonline.com/loi/ueqe20

Seismic Retrofitting of Non-Seismically Designed RC Beam-Column Joints using Buckling Restrained Haunches: Design and Analysis

Bin Wang, Songye Zhu, You-Lin Xu & Huanjun Jiang

To cite this article: Bin Wang, Songye Zhu, You-Lin Xu & Huanjun Jiang (2017): Seismic Retrofitting of Non-Seismically Designed RC Beam-Column Joints using Buckling Restrained Haunches: Design and Analysis, Journal of Earthquake Engineering, DOI: 10.1080/13632469.2016.1277441

To link to this article: http://dx.doi.org/10.1080/13632469.2016.1277441

Accepted author version posted online: 31 Jan 2017.

Seismic Retrofitting of Non-Seismically Designed RC Beam-Column Joints using Buckling Restrained Haunches: Design and Analysis

Bin WANG[1], Songye ZHU[1*], You-Lin XU[1], and Huanjun JIANG[2]

[1]Department of Civil and Environmental Engineering, The Hong Kong Polytechnic University, Hong Kong, China

[2]State Key laboratory of Disaster Reduction in Civil Engineering, Tongji University, Shanghai, China

Abstract

Many existing RC structures around the world were designed to sustain gravity and wind loads only. Past earthquake reconnaissance have shown that strong earthquakes can lead to substantial damage ranges to non-seismically designed RC buildings, particularly to beam-column joints. This paper presents a novel retrofit method using buckling restrained haunches (BRHs) to improve the seismic performance of such joints. A numerical model for RC joints is introduced and validated. Subsequently, a new seismic retrofit strategy using BRHs is proposed, aimed at relocating plastic hinges and increasing energy dissipation. The results indicate the retrofit method can effectively meet the performance objectives.

[*]Address correspondence to Songye Zhu, Department of Civil and Environmental Engineering, The Hong Kong Polytechnic University, Hong Kong, China; E-mail: ceszhu@polyu.edu.hk

Keywords Non-Seismically Designed RC Beam-Column Joint; Buckling Restrained Haunches; Plastic Hinge Relocation; Seismic Retrofit; Energy Dissipation

Article History

Received 23 September 2016

Accepted 10 December 2016

1. Introduction

Seismic safety of a large number of existing non-seismically designed reinforced concrete (RC) structures is a major concern around the world. Evidences from past earthquake reconnaissance (Northridge 1994, Kobe 1995, Kocaeli 1999, Christchurch 2011) demonstrated that non-seismically designed RC buildings are vulnerable to substantial damage or even collapse under moderate to severe earthquakes. In general, non-seismically designed RC structures can be classified into two categories: one has the construction time prior to the introduction of seismic design provisions with ductility concept, such as the buildings constructed in California before the mid-1970s according to the 1967 Uniform Building Code [Liel *et al*., 2011]; the other is in regions of low-to-moderate seismicity where structures were traditionally designed with no or little consideration of seismic resistance, such as Hong Kong and Singapore whose design philosophy had followed the British standard BS8110 for a long time [Kuang and Wong, 2006; Pam and Ho, 2010; Li and Pan, 2007]. Buildings designed and detailed taking into account only gravity and wind loads would have to rely greatly on its

inherent ductility if a severe earthquake were to strike.

Non-seismically designed structures mainly feature inadequate reinforcement details, such as a lack of joint transverse reinforcement, insufficient transverse reinforcement in columns, column lap splice located in potential plastic hinge regions, and inadequate anchorage detailing [NIST, 2013]. Typical reinforcement details of non-seismically designed beam-column interior and exterior joints are shown in Fig. 1. In this paper, the deficiencies in beam-column joints are of particular interest because they are likely to fail prior to the formation of plastic hinges in the beams, thereby leading to the severe deterioration or premature collapse of buildings. For these reasons, ACI-ASCE Committee 352 stated that methods for improving the performance of older joints need to be studied because only limited knowledge was available on connection repair and retrofitting [ACI-ASCE Committee 352, 2002].

To improve the seismic capacity of non-seismically designed beam–column joints, a variety of strengthening and retrofit techniques have been studied and adopted to improve joint performance in practice. The most common retrofit solutions involve strengthening the joints themselves and improving joint shear resistance capacity, using such as jacketed fibre reinforced polymers [Ghobarah and Said, 2001], externally bonded steel plate [Sasmal *et al*., 2011], and increasing joint sections [Karayannis *et al*., 2008]. Alternatively, retrofitting that changes the force distribution in the joint assemblage and reduces shear stress in joints has received interest for seismic retrofit of non-seismically designed beam–column joints in the past decade, such as

adding metallic haunch [Pampanin *et al*., 2006], steel bracing [Said and Nehdi, 2008; Sharbatdar *et al.*, 2012], and steel angles [Shafaei *et al.*, 2014]. Compared with the former strengthening techniques, these retrofit measures result in relatively low-damage solutions and are easy to install in practice. In addition, buckling-restrained braces (BRBs), as an ideal combination of structural members and hysteretic dampers, have been proposed to retrofit the entire RC frames by researchers [Di Sarno and Manfredi, 2010, 2012; Sutcu *et al*., 2014; Mahrenholtz *et al*., 2015].

The paper investigates a novel seismic retrofit solution by using a device termed buckling restrained haunches (BRHs), which sustains a pure axial load when connected to the adjacent components through pinned connections. BRH solutions provide both bracing function and reliable energy dissipation capacity for the strengthening of RC joints subjected to seismic cyclic loading. This study first presents the proof-of-concept experiment of a scaled BRH specimen and the numerical modelling approach for non-seismically designed beam-column joints. Subsequently, a design methodology for the seismic retrofitting of non-seismically designed beam–column joints using BRHs is proposed and validated by numerical analyses of two representative cases. Compared with the original non-seismic RC joints, the retrofitted joints demonstrate significantly enhanced seismic performance in terms of strength, ductility, and energy dissipation. The analysis results indicate the effectiveness of the proposed retrofit method using BRHs in meeting the expected target of the design procedures.

2. Scaled BRHs Test

Described in this section are the design and BRH experimental results. BRHs are essentially short versions of BRBs that can carry compression load without buckling and exhibit nearly symmetric yield behaviour under tension and compression. As shown in Fig. 2(a), the BRH consists of a steel core (energy dissipating bar), a buckling restraining case that provides lateral restraint against the core buckling, and the debonding material or gap that reduces the friction between the buckling restraining case and the steel core. The BRH is designed to resist axial forces only and to exhibit stable energy dissipation without any strength degradation. In particular, it is expected that the inelastic deformation and energy dissipation is concentrated in the reduced-diameter segment and that other parts and connections remain essentially elastic. Thus, the relationship of the reduced diameter d_E of the energy dissipating bar and the diameter d_V of the virgin bar can be expressed as [Guerrini *et al*., 2015]:

$$d_E \le d_V \times \sqrt{\frac{f_{E,y}}{f_{E,\mathrm{u}}}} \qquad (1)$$

where $f_{E,y}$ and $f_{E,u}$ are the yield and ultimate strengths of the energy dissipation bar, respectively.

Fig. 2(b) shows a scaled BRH fabricated and assembled in laboratory. Austenite stainless steel was used in the scaled BRHs. The reduced section energy dissipating part of the bar has a length of L_E=100mm, and the diameters of the reduced and original sections are d_E = 6mm and

d_V = 10mm, respectively. The measured yield stress and elastic modulus are 605MPa and 194GPa, respectively.

Cyclic tests on the scaled BRH specimen were carried out to validate its hysteretic behaviour. Fig. 2(c) shows the BRH specimen under test on an MTS machine (uniaxial tension/compression test machine). Fig. 3 shows the load-deformation relationships obtained from the experiment of the BRH specimen, in which satisfactory hysteretic behaviour without any strength and stiffness degradation is obtained. Moreover, the Steel02 material model in OpenSees [Mazzoni *et al*., 2006], which employs Giuffré-Menegotto-Pinto Material model with isotropic strain hardening, is used to reproduce the BRH hysteretic response. The hysteretic parameters of the Steel02 model are: b=0.015, R_0=16, cR_1=0.9, cR_2=0.15, a_1=0.03, a_2=0.9, a_3=0.01, a_4=1.0. A good agreement between the experimental and simulation results can be observed, indicating that this model provides a good representation of BRH behaviour.

3. Non-seismically designed beam-column joint behaviour

There is a consensus that a RC frame under earthquakes can result in relatively high shear stress and bond stress in the joints. These stresses may lead to local deformation and nonlinear response in joint zones, especially in the case of non-seismically designed beam-column joints. The joint deformations under lateral loads mainly involve the following two effects: (1)

reinforcing bar slip in beam and column; and (2) joint shear distortion [Moehle, 2014].

Due to the absence of capacity design considerations, different potential failure modes in the interior and exterior joints with non-seismic details may occur, depending on the reinforcement details [Elnashai and Di Sarno, 2015]. Typical damage modes of joint shear failure and anchorage failure for beam bottom reinforcement with inadequate embedment length are shown in Fig. 4. These local damage mechanisms are prone to result in rapid strength degradation of the lateral resistance system. Accurately predicting the behaviour of non-seismically designed joints is essential to assess seismic performance and retrofit design.

4. Numerical model of non-seismically designed beam-column joint

There are two existing joint analytical models in OpenSees, and the corresponding elements are called “BeamColumnJoint Element” and “Joint2D Element”. These models, however, were not adopted in this study because the multiple nodes or springs involved in these models may affect numerical robustness and efficiency.

Fig. 5 presents the numerical models of interior and exterior joint assemblages used in this study. To describe nonlinear shear behaviour in the joint, the model proposed by Alath and Kunnath [1995] was employed in this study. Columns and beams in the joint assemblage are modelled using the force-based beam-column element with fibre sections, which are divided into

the unconfined zone and confined zone to take the effect of hoops into account. The constitutive relationship used to describe unconfined concrete and confined concrete follows the "Concrete02" model in OpenSees. The corresponding stress and strain values at the peak and the crushing point of confined concrete are calculated using the Chang and Mander model [1994]. Longitudinal reinforcement is represented using the "Steel02" model. The zero-length slip spring adopted to model the bar slip effect at the interface of beam-column joint is discussed in Sec. 4.1. Joint rotation spring is modelled using "Pinching4" material. The envelope and hysteresis rules are defined in Sec. 4.2. The joint size is represented by four rigid links shown in Fig. 5.

4.1 Bar slip model for interface of joints

As mentioned in Section 3, the bar-slip deformation at the interface of beam-column joint is one source of joint deformation. The moment at the end of a beam tends to cause tension in the longitudinal rebar, as shown in Fig. 6. The tension force must be resisted by the bond stress, u, between the rebar and the concrete, which is assumed to be constant along the anchored length under external loading.

Zero-length slip springs are modelled at the interface to simulate the deformation associated with bar slip, as shown in Fig. 5. The rotational stiffness of the spring, k_{slip}, is calculated following the recommendations of Elwood and Eberhard [2009]:

$$k_{slip} = \frac{8u}{d_b f_s} EI_{flex} \qquad (2)$$

where u is the uniform bond stress ($0.8\sqrt{f_c}$ MPa); d_b is the diameter of the longitudinal reinforcement (mm); f_s is the stress in the tension rebar and its maximum value can be taken as the yield stress of the longitudinal rebar (MPa); EI_{flex} is the effective flexural rigidity ($0.4EI_{gross}$); E denotes the modulus of elasticity of concrete (MPa); and I_{gross} is the gross section moment of inertia (mm^4).

4.2 Shear strength model for exterior and interior joints

The shear deformation of joint is modelled using zero-length rotational spring with the same node coordinates at the centre of the joint (the intersection of beam and column centrelines), as shown in Fig. 5. The two nodes are connected to the column rigid link and beam rigid link, respectively. The joint shear stress-strain relationship (τ_j-γ_j) can be converted into the moment-rotation relationship (M_j-θ_j) as provided in Celik and Ellingwood [2008]:

$$M_j = \tau_j A_j \frac{1}{(1-h_c/L_b)\,jd - 1/L_c} \quad (3)$$

$$\theta_j = \gamma_j \quad (4)$$

where τ_j is the joint shear stress and A_j is the joint area, calculated according to ACI 318 [2014]; h_c is the depth of column; L_b and L_c are the total length of the beams and columns, respectively; jd denotes the internal moment arm of the beam; θ_j is the rotation of the spring; and γ_j is the joint shear strain.

The joint rotational springs of exterior and interior joints are represented using Pinching4 material. The response envelop of joints is shown in Fig. 7, which can be described by four characteristic points: (1) Cracking strength point (τ_c-γ_c); (2) Yielding point (τ_y-γ_y); (3) Peak strength point (τ_{max}-γ_p); and (4) Residual strength point(τ_r-γ_r). Joint shear stress and strain of different characteristic point for both exterior and interior joints are defined in Table 1.

A reasonable prediction of shear strength, τ_{max}, is essential for assessing the seismic capacity of non-seismically designed beam-column joints. Several empirical and analytical models for joint shear strengths have been proposed by researchers previously [Priestley, 1997; Jeon *et al*., 2015; Anderson *et al*., 2008; Ning *et al*., 2016]. In this study, the shear strength model is based on the principal tensile stress concept; meanwhile, the effect of beam–column depth ratio is taken into account (the equation is given in Table 1). The beam–column depth ratio, h_b/h_c, has a significant effect on the strength and ductility of beam–column joints [Wong and Kuang, 2008]. The effect of the joint aspect ratio on joint shear strength can be explained by the strut and tie approach where a steeper diagonal strut is developed in the high aspect ratio of a joint region and such a steeper strut is less effective in resisting the horizontal joint shear force [Park and Mosalam, 2013].

4.3 Modelling results and validation

Experimental results of typical exterior and interior non-seismically designed joints with different design parameters are considered to validate the numerical model, including an exterior joint with conventional reinforcement type (Specimen BS-L [Kuang and Wong, 2006]), an exterior joint with one bend away bar (Specimen BS-LL [Kuang and Wong, 2006]), and interior joints with conventional reinforcement type (Specimen E-0.3 [Au *et al*., 2005] and PEER14 [Walker, 2001]). None of the joint specimens had transverse reinforcement and they did not meet the modern seismic design codes; consequently, they have shown joint failure mode under the cyclic loading.

Fig. 8 shows a comparison of the force-displacement hysteretic relationship between the experimental and numerical results. In general, there is good agreement between the experimental and numerical behaviour for the specimens with different design parameters and reinforcement details. The numerical model is able to capture the loading and unloading behaviours, including the stiffness and pinch hysteretic behaviour. Moreover, the peak strengths of test results are well predicted by the shear strength model introduced in this study.

5. Approach and design of seismic retrofit using BRHs

5.1 Seismic retrofit approach

The absence of seismic design resulted in poor performance of RC components (e.g., joint and column) in many existing buildings, which are not able to develop the expected capacity to meet seismic demand when subjected to potential earthquakes. Most common retrofit techniques focused on the strength of the non-seismically designed joints and aimed to improve the joint shear strength in the retrofit design. As a result, new weak points (locations for damage) may potentially transfer to the adjacent non-ductile columns or beams since the strength proportion of these components had been changed, which would lead to adverse damage to the non-ductile columns or beams as well. An ideal seismic retrofit strategy for existing buildings would not only protect non-seismically designed beam-column joints, but also further improve structures to exhibit the desired damage modes and energy dissipation mechanism.

Local retrofit methods, such as the addition of metallic haunches, steel bracing, or steel angles, change the force distribution in beam-column joint assemblages and improve seismic performance by protecting against joint shear failure by forming plastic hinges in beams in new locations. In this paper, a new retrofit method with the installation of BRHs in beam-column joint assemblages is proposed, as shown in Fig. 9. Short BRHs are proposed to be installed at the beam-column joints regarded as an ideal combination of structural members and yielding

dampers. They are hinge-connected to the RC frames so as to achieve purely axial behaviour. BRHs can redistribute loads within the joint region and enhance energy dissipation under large joint deformation.

5.2 Retrofit design procedures

To understand the behaviour of beam-column joints retrofitted with BRHs, it is important to explain the effect of redistributing the shear forces and moments in the joints. The geometric parameters (distance L, and angle α) and the BRH yield strength F_y, all affect the internal force distribution in the joint subassembly. Fig. 10 shows the internal force distribution for retrofitted exterior joint with BRHs. The joint shear force V_{hj} can be obviously reduced by the BRHs and the maximum moment in the beam and column is relocated from the beam-column interface to the BRHs intersection point. There is a moment reduction at the BRH intersection point, because of its offset from the centreline intersection point of the joint.

The retrofit objective is to prevent shear failure of non-seismically designed RC joints and re-locate flexural plastic hinges into the beams. Such performance objective allows extensive damage in beams but slight damage in columns and joints (e.g. spalling of cover in columns and minor cracks at joint). Based on the acceptable performance target, three parameters, namely, L, α and F_y, are chosen using the following procedure:

(1) To prevent joint shear failure, the joint shear stress τ_{hj} should not exceed τ_{max} defined in

Table 1:

$$\tau_{hj}^{'} = \frac{V_{hj}^{'}}{A_j} \le \tau_{\max} \quad (5)$$

(2) To form plastic hinges in beams, the maximum moment, $M_b^{'}$, at the intersection with the beam in the retrofit joint subassembly should reach the yielding moment $M_{b\text{-}yield}$, while the corresponding shear force, $V_b^{'}$, should not exceed the shear strength of beam based on ACI318 [2014]:

$$V_b^{'} = \frac{M_{b-yield}}{L_b/2 - h_c/2 - L} < V_n^b = 0.17\lambda\sqrt{f_c}\, b_w d + \frac{A_v f_{yt} d}{s} \quad (6)$$

where λ is 0.75 and 1.0 for light and normal weight aggregate concrete, respectively; b_w is the beam width; d is the effective depth; A_v is the area of transverse reinforcement; f_{yt} is the yield stress of transverse reinforcement; s is the spacing of transverse reinforcement.

(3) To avoid the plastic hinge and shear failure in columns, the maximum moment, $M_{tc}^{'}$, at the intersection with the column in the retrofit joint subassembly should not reach the yielding moment $M_{c\text{-}yield}$. The corresponding shear force, $V_{tc}^{'}$ or $V_{bc}^{'}$, should not exceed the shear strength of column based on ASCE/SEI 41-06 [2007]:

$$V_{tc}^{'}, V_{bc}^{'} = \frac{M_{c-yield}}{L_c/2 - h_b/2 - L\tan\alpha} < V_n^c = k\left(\frac{0.5\lambda\sqrt{f_c}}{M/(Vd)}\sqrt{1 + \frac{N_u}{0.5\sqrt{f_c}A_g}}\right)0.8A_g + \frac{A_v f_{yt} d}{s} \quad (7)$$

$$M_{tc}^{'}, M_{bc}^{'} = M_{b-yield} \frac{L_b(L_c/2 - h_b/2 - L\tan\alpha)}{L_c(L_b/2 - h_c/2 - L)} < M_{c-yield} \quad (8)$$

where *M/Vd* is the largest ratio of moment to shear, multiplied by the effective depth($2 \leq M/Vd \leq 4$); N_u is the axial compression load; A_g is the gross cross-sectional area, k is the factor related to displacement ductility demand and can be taken as 1 for the purpose of calculating column shear strength.

This seismic retrofit design involves the adjustment of the three parameters (namely, L, α and F_y) to satisfy the equations (5), (6), (7) and (8). The design flowchart for non-seismic RC joints retrofitted with BRHs is shown in Fig. 11. Although the design process is introduced on the basis of an exterior joint shown in Fig. 10, it is also applicable to interior joints.

6. Case study and numerical validation

6.1 Exterior joint

Kuang and Wong [2006] tested five full-scale RC exterior beam-column joints, which were the representative joints in the frames designed according to BS8110 code [1997] under cyclic loading. The results indicated that shear failure of the joints occurred before the beam section reached its ultimate flexural strength. In fact, the inadequate design of the joint details may lead to unexpected damage of RC frame buildings during low-to-moderate earthquakes. Specimen BS-L shown in Fig. 8(a), was selected to illustrate the effectiveness of the proposed retrofit

strategy. Fig. 12(a) gives the specimen dimensions and reinforcement details. The experimental parameters are: f_c=30.9MPa, f_y=520.0MPa, f_{yt}=500.0MPa, and the axial compression ratio of column μ=0.15. The retrofit design is as follows:

(1) Calculation of τ_{max} as explained in Table 1: τ_{max}=3.1MPa.

(2) Calculation of $M_{b\text{-}yield}$ using the moment-curvature method for beam: $M_{b\text{-}yield}$=200.1kN.m; Calculation of V_n^b using Eq.(6):

$$V_n^b = 0.17\lambda\sqrt{f_c}b_w d + \frac{A_v f_{yt} d}{s} = 232.3\,\text{kN}$$

$$V_b^{'} = \frac{M_{b-yield}}{L_b/2 - h_c/2 - L} = \frac{200.1}{1.45 - 0.15 - L} < V_n^b = 232.3,\ L<0.43\text{m}.$$

(3) Calculation of $M_{c\text{-}yield}$ using the moment-curvature method for column: $M_{c\text{-}yield}$=174.1kN.m; Calculation of V_n^c using Eq.(7):

$$V_n^c = \left(\frac{0.5\lambda\sqrt{f_c}}{M/(Vd)}\sqrt{1+\frac{N_u}{0.5\sqrt{f_c}A_g}}\right)0.8A_g + \frac{A_v f_{yt} d}{s} = 196.7\,\text{kN}$$

$$V_{tc}^{'}, V_{bc}^{'} = \frac{M_{c-yield}}{L_c/2 - h_b/2 - L\tan\alpha} = \frac{174.1}{1.45 - 0.225 - L\tan\alpha} < V_n^c = 196.7\,\text{kN},\ L\tan\alpha < 0.34\text{m}.$$

(4) To guarantee a plastic hinge will not form in the column by Eq.(8):

$$M_{tc}^{'}, M_{bc}^{'} = 200.1\times\frac{2.9\times(1.45 - 0.225 - L\tan\alpha)}{2.9\times(1.45 - 0.15 - L)} < M_{c-yield} = 174.1\,\text{kN.m}$$

Based on the above discussion, the assumed design parameters are L=300mm, α=50°,

$f_{y,BRH}$=235MPa and $A_{s,\,BRH}$=1400mm^2. The corresponding BRH yield strength F_y is 329kN.

6.2 Interior joint

Walker [2001] tested seven RC interior beam-column joints, which were representative of frames constructed prior to 1970, under reversed cyclic loading. None of these specimens contained transverse shear reinforcement in the panel zone. Specimen PEER-14 was selected to illustrate the retrofit effectiveness. Fig. 12(b) shows the specimen dimensions and reinforcement details. The experimental parameters are: f_c=31.7MPa, $f_{y,\#7}$=422.6MPa, $f_{y,\#6}$=427.5MPa, $f_{yt,\#4}$=661.9MPa, and the axial compression ratio of column μ=0.1.

(1) Calculation of τ_{max} as explained in Table 1: τ_{max}=5.8MPa.

(2) Calculation of $M_{b\text{-}yield}$ using the moment-curvature method for beam: $M_{b\text{-}yield}$=230.3kN.m; Calculation of V_n^b using Eq.(6):

$$V_n^b = 0.17\lambda\sqrt{f_c}b_w d + \frac{A_v f_{yt} d}{s} = 1498.2\ \text{kN}$$

$$V_b^{'} = \frac{M_{b-yield}}{L_b/2 - h_c/2 - L} = \frac{230.3}{1.83 - 0.23 - L} < V_n^b = 1498.2\ \text{kN},\ L<1.45\text{m}$$

(3) Calculation of $M_{c\text{-}yield}$ using the moment-curvature method for column: $M_{c\text{-}yield}$=362.2kN.m; Calculation of V_n^c using Eq.(7):

$$V_n^c = \left(\frac{0.5\lambda\sqrt{f_c}}{M/(Vd)}\sqrt{1+\frac{N_u}{0.5\sqrt{f_c}A_g}}\right)0.8A_g + \frac{A_v f_{yt} d}{s} = 1328.7\ \text{kN}$$

$$V_{tc}^{'}, V_{bc}^{'} = \frac{M_{c-yield}}{L_c/2 - h_b/2 - L\tan\alpha} = \frac{362.2}{1.07 - 0.25 - L\tan\alpha} < V_n^c = 1328.7\,\text{kN}, L\tan\alpha < 0.55\text{m}$$

(4) To guarantee the plastic hinge will not form in column by Eq.(8):

$$M_{tc}^{'}, M_{bc}^{'} = 230.3 \times \frac{3.66 \times (1.07 - 0.25 - L\tan\alpha)}{2.13 \times (1.83 - 0.23 - L)} < M_{c-yield} = 362.2\,\text{kN.m}$$

Based on the above discussion, the assumed design parameters are L=400mm, α=45°, $f_{y,BRH}$=235MPa and $A_{s,\,BRH}$=960mm^2. The corresponding yield strength F_y of BRHs is 226kN.

6.3 Simulation results

6.3.1 Hysteretic behaviour

The numerical models of the two retrofitted beam-column joints were similar to those introduced in Sec. 4. The BRHs were modelled as pin-ended truss members using the "Steel02" material, which has been validated by the BRH test in Section 2. The cross-sectional areas of these elements were equal to the core area of the BRHs designed above.

The loading protocols used in the tests of BS-L and PEER14 specimens are shown in Fig. 13. The loading protocols using displacement control typically consisted of two or three cycles at each level and the loading displacement amplitude increased until failure. The corresponding inter-story drift ratios are also shown in Fig. 13. The maximum displacement is greater than of 4% inter-story drift ratio, and this level corresponds to the "Collapse Prevention" performance level of RC frames [ASCE/SEI 41-06, 2007]. To compare the improved hysteretic behaviour of the

retrofitted specimens with the original ones, the same cyclic loading histories were employed in the numerical study.

The hysteretic behaviour of the two retrofitted specimens is shown in Fig.14. The behaviour of the original (i.e., un-retrofitted) joints are also overlapped. The comparisons indicate that the cyclic behaviour of the retrofitted joints with proposed BRHs is improved significantly. Compared with the original joints, the yield load capacity of the retrofitted BS-L and PEER14 specimens was increases by around 3.1 and 1.6 times, respectively; and their initial stiffness was increased by 4.2 and 5.1 times, respectively. Shear failure in the joints of original specimens led to relatively low load carrying capacity, non-ductile behaviour, and significantly pinch response of hysteretic curves. In contrast, load carrying capacity, ductility and energy dissipation of the retrofitted joints were considerably higher than those of the original specimens, which are attributed to the load redistribution among different components (the joints and beams) and the contribution of BRHs.

6.3.2 Joint shear stress

The behaviour of the retrofitted joints is further illustrated by the stress-strain responses shown in Fig. 15 and Fig. 16. The maximum shear stresses in the retrofitted BS-L and PEER14 joints are 2.8MPa and 3.6MPa, respectively. Both are lower than the stresses in the original specimens. Moreover, the maximum shear strains of the retrofitted BS-L and PEER14 joints are

0.006 and 0.0033 over the whole of the cyclic loading, respectively, which is considerably decreased by 82.8% and 93.2%, respectively, in comparison with the original specimens. In addition, due to the load redistribution between the joints and beams, the plastic hinges are relocated further away from the joint, which consequently reduce the stress and strain in the joints.

6.3.3 Damage modes

The damage modes of retrofitted specimens are shown in Fig. 17. For the retrofitted BS-L joint, the maximum longitudinal reinforcement strains in the beam and column were 0.1 and 0.001, respectively. For the retrofitted PEER14 joint, the maximum longitudinal reinforcement strain in the beam and column were 0.12 and 0.0008, respectively. According to the strain limits defined for various limit states in [Kowalsky, 2000], column repair would not be needed after the earthquake, while extensive damage does occur in beams. The final damage states of the beams and columns are also depicted in Fig. 16. It implies that the plastic hinges develop in the beams at the haunch intersections instead of in the columns; meanwhile, shear failure in the joints is avoided. Both outcomes conform to retrofitting objectives.

6.3.4 Energy dissipation

Energy dissipation capacity is one of the most important criteria for assessing the seismic performance of a component when subjected to cyclic loading. BRHs are designed to relocate plastic hinges and offer supplementary energy dissipation in this proposed retrofit method. It will redistribute the internal force around the joint region like a steel bracing and prevent the shear damage of the RC joint. In addition, it functions as a damper dissipating energy under load reversal conditions. The axial BRH force-displacement relationships in the two retrofitted joints are shown in Fig. 18. The BRHs in the retrofitted BS-L joint yielded at the displacements of 5.1mm (i.e., 0.4% inter-story drift), while the beam yielded at the displacement of 14.8mm (i.e., 1.2% inter-story drift). Similarly, the BRHs in the retrofitted PEER14 joint yielded at the displacement of 5.7mm (i.e., 0.3% drift), while the beam yielded at the displacement of 7.7mm (i.e., 0.4% drift). The fat hysteresis of the BRHs indicates that the BRHs not only enhanced the stiffness and strength of the retrofitted joints, but also served as energy dissipating dampers. The BRHs started to dissipate the energy before the plastic hinges formed in the beams. The equivalent damping ratio of BRHs in two specimens ranges from 10%~30% approximately.

Fig. 19 shows the comparison of the cumulative energy dissipation curves for the two cases. Strain energy consists of elastic and inelastic parts, where the former is conservative and becomes zero upon unloading while the latter is dissipative. Thus, the energy dissipated in each loading cycle is computed as the area enclosed by the corresponding hysteresis loop shown in

Fig. 14. The energy dissipation capacity of the original joints mainly depends on the shear damage of the joints. For the BRH retrofitted specimens, however, the inelastic deformation of both the beams and the BRHs are the main sources of the energy dissipation capacity. The retrofitted specimens dissipate considerably more energy in comparison with the original specimens, and the energy dissipation is amplified by around thirteen and six times, respectively, in the retrofitted specimens BS-L and PEER14. The portions of energy dissipation by BRHs in the retrofitted specimens BS-L and PEER14 account for 18.1% and 10.1%, respectively. Meanwhile, the portions of energy dissipation by plastic hinges in beams of BS-L and PEER14 are 81.9% and 89.9%, respectively.

Seismic input energy to a structure is equal to the sum of structural kinetic energy, inherent damping energy, elastic strain energy and dissipative hysteretic energy [Uang and Bertero, 1990; Akiyama, 1988]. The kinetic and inherence damping energy is absent in the presented quasi-static experiments. Thus, the components of energy dissipation are mainly the dissipative hysteretic energy of the beams and BRHs. The enhanced joint energy dissipation will lead to the reduced peak displacement responses under earthquakes. Such a benefit is not apparent in the cyclic tests with the fixed displacement protocols and needs to be further illustrated through the seismic analyses of entire RC frames retrofitted by BRHs in future studies.

7. Conclusions

This paper proposes a novel seismic retrofitting method using BRHs for typical non-seismically designed RC joints. This seismic retrofit method is based on the concept of relocating plastic hinges into beams and increasing energy dissipation under earthquakes. A proof-of-concept test on a reduced scale BRH specimen was conducted and test results indicated that the proposed BRH provides stable energy dissipation capacity, in addition to bracing action, under cyclic loading. A seismic retrofit design methodology for non-seismically designed beam–column joints using BRHs is proposed, and its effectiveness is validated by numerical simulations of two representative cases. Compared with the original non-seismically designed RC joints, the retrofitted joints demonstrate significantly enhanced seismic performance in terms of strength, ductility, and energy dissipation. This is attributed to the load redistribution among different components (i.e., the joints and beams) and the contribution of BRHs. Due to the load redistribution between the joints and beams, plastic hinges are relocated further away from the joint, which consequently reduced the stress and strain in the joints. Damage modes imply that the plastic hinges develop in the beams at the haunch intersection instead of in the columns, and meanwhile shear failure of the joints is avoided, which satisfactorily achieves the retrofit objective.

It is to be noted that the BRH design parameters of this study do not represent an optimal design for the retrofitted specimen. An optimal design, as such, was not the purpose of the study.

It would be possible to optimize the design based on the retrofitted target. The retrofit technique introduced here is regarded as a local strengthening method focusing on damage control in the joint subassembly. The local and global retrofit strategies may be combined in engineering practice to consider different retrofit performance levels for joints and other components.

Acknowledgments

The authors are grateful for the financial support provided by The Hong Kong Polytechnic University (Project No. 4-ZZCG) and by the Innovation and Technology Commission of the HKSAR Government to the Chinese National Engineering Centre for Steel Construction (Hong Kong Branch). The findings and opinions expressed in this paper are solely those of the authors and do not represent the views of the sponsors.

References

ACI Committee 318. [2014]. "Building code requirements for structural concrete (ACI 318–14)," American Concrete Institute, Farmington Hills, Michigan.

ACI-ASCE Committee 352. [2002] "Recommendations for design of beam–column joints in monolithic reinforced concrete structures (ACI 352R-02)," American Concrete Institute, Farmington Hills, Michigan.

Akiyama, H. [1988] "Earthquake Resistant Design Based on the Energy Concept," Proceedings

of The Ninth World Conference on Earthquake Engineering, Tokyo-kyoto, Japan, pp. 905-910.

Alath, S. and Kunnath, S. K. [1995] "Modeling inelastic shear deformation in reinforced concrete beam-column joints engineering mechanics," 10th Conf. on Engineering Mechanics, University of Colorado at Boulder, Colorado, USA, pp. 822–825.

Anderson, M., Lehman, D., and Stanton, J. [2008] "A cyclic shear stress–strain model for joints without transverse reinforcement," *Engineering Structures*, **30**(4), 941-954.

ASCE/SEI Seismic Rehabilitation Standards Committee. [2007] "Seismic Rehabilitation of Existing Buildings (ASCE/SEI 41-06)," American Society of Civil Engineers, Reston, VA.

Au, F. T. K., Huang, K., and Pam, H. J. [2005] "Diagonally-reinforced beam-column joints reinforced under cyclic loading," *Proceedings of the Institution of Civil Engineers-Structures and Buildings*, **158**(1), 21-40.

BS 8110. [1997] "Structural Use of Concrete- Part 1: Code of Practice for Design and Construction," BSI, London.

Celik, O. C. and Ellingwood, B. R. (2008). "Modeling beam-column joints in fragility assessment of gravity load designed reinforced concrete frames," *Journal of Earthquake Engineering*, **12**(3), 357-381.

Chang, G. A. and Mander, J. B. [1994]. "Seismic Energy Based Fatigue Damage Analysis of Bridge Columns: Part I – Evaluation of Seismic Capacity". Technical Report NCEER-94-0006,

Multidisciplinary Center for Earthquake Engineering Research, University at Buffalo, New York.

Di Sarno, L. and Manfredi, G. [2010]. "Seismic retrofitting with buckling restrained braces: Application to an existing non-ductile RC framed building." *Soil Dynamics and Earthquake Engineering*, 30(11), 1279-1297.

Di Sarno, L. and Manfredi, G. [2012]. "Experimental tests on full-scale RC unretrofitted frame and retrofitted with buckling-restrained braces." *Earthquake Engineering & Structural Dynamics*, 41(2), 315-333.

Elnashai, A. S. and Di Sarno, L. [2015]. Fundamentals of Earthquake Engineering: From Source to Fragility (2nd Edition). John Wiley & Sons, Inc., New York.

Elwood, K. J. and Eberhard, M. O. [2009] "Effective Stiffness of Reinforced Concrete Columns," *ACI Structural Journal,* **106**(4), 476-484

Ghobarah, A. and Said, A. [2001]. "Seismic rehabilitation of beam-column joints using FRP laminates". *Journal of Earthquake Engineering*, 5(1), 113-129.

Guerrini, G., Restrepo, J. I., Vervelidis, A., and Massari, M. [2015] "Self-centering precast concrete dual-steel-shell columns for accelerated bridge construction: seismic performance, analysis, and design," Technical Report 2015/13, Pacific Earthquake Engineering Research Center, University of California, Berkeley, California.

Jeon, J. S., Lowes, L. N., DesRoches, R., and Brilakis, I. [2015] "Fragility curves for non-ductile reinforced concrete frames that exhibit different component response mechanisms," *Engineering Structures*, **85**, 127-143.

Karayannis, C. G., Chalioris, C. E., and Sirkelis, G. M. [2008] "Local retrofit of exterior RC beam-column joints using thin RC jackets-An experimental study," *Earthquake Engineering & Structural Dynamics*, **37**(5), 727-746.

Kowalsky, M. J. [2000] "Deformation limit states for circular reinforced concrete bridge columns," *Journal of Structural Engineering*, **126**(8), 869-878.

Kuang, J. S., and Wong, H. F. [2006] "Effects of beam bar anchorage on beam-column joint behaviour," *Proceedings of the Institution of Civil Engineers-Structures and Buildings*, **159**(2), 115-124.

Li, B. and Pan, T. C. [2007] "Seismic behavior of non-seismically detailed reinforced concrete structural systems and components-What have we been learning?" *Journal of Earthquake and Tsunami*, **1**(2), 139-159.

Liel, A. B., Haselton, C. B., and Deierlein, G. G. [2011] "Seismic Collapse Safety of Reinforced Concrete Buildings. II: Comparative Assessment of Nonductile and Ductile Moment Frames," *Journal of Structural Engineering*, **137**(4), 492-502.

Mazzoni, S., McKenna, F., Scott, M. H., and Fenves, G. L. [2006]. "OpenSees command

language manual," Pacific Earthquake Engineering Research Center. University of California, Berkeley.

Mahrenholtz, C., Lin, P. C., Wu, A. C., Tsai, K. C., Hwang, S. J., Lin, R. Y. and Bhayusukma, M. Y. [2015]. "Retrofit of reinforced concrete frames with buckling-restrained braces." *Earthquake Engineering & Structural Dynamics*, 44(1), 59-78.

Moehle J. [2014]. Seismic Design of Reinforced Concrete Buildings. McGraw-Hill Education, New York.

Ning, C. L., Yu, B., and Li, B. [2016] "Beam-Column Joint Model for Nonlinear Analysis of Non-Seismically Detailed Reinforced Concrete Frame," *Journal of Earthquake Engineering*, **20**(3), 476-502.

NIST. [2013] "Review of Past Performance and Further Development of Modeling Techniques for Collapse Assessment of Existing Reinforced Concrete Buildings," NIST GCR-14-917-28, NEHRP Consultants Joint Venture, Gaithersburg, Maryland.

Pantelides, C.P., Hansen, J., Nadauld, J., and Reaveley, L. D. [2002]. "Assessment of Reinforced Concrete Building Exterior Joints with Substandard Details," Pacific Earthquake Engineering Research Center, PEER Report, University of California, Berkeley.

Pam, H. J. and Ho, J. C. M. [2010] "Effects of Steel Lap Splice Locations on Strength and Ductility of Reinforced Concrete Columns," *Advances in Structural Engineering*, **13**(1),

199-214.

Pampanin, S., Christopoulos, C., and Chen, T. H. [2006] "Development and validation of a metallic haunch seismic retrofit solution for existing under-designed RC frame buildings," *Earthquake Engineering & Structural Dynamics*, **35**(14), 1739-1766.

Park, S. and Mosalam, K. M. [2013] "Simulation of reinforced concrete frames with nonductile beam-column joints," *Earthquake Spectra*, 29(1), 233-257.

Priestley, M. J. N. [1997]. "Displacement-based seismic assessment of reinforced concrete buildings," *Journal of earthquake Engineering*, **1**(1), 157-192.

Said, A. and Nehdi, M. [2008] "Rehabilitation of RC frame joints using local steel bracing," *Structure and Infrastructure Engineering*, **4**(6), 431-447.

Sasmal, S., Ramanjaneyulu, K., Novak, B., Srinivas, V., Kumar, K. S., Korkowski, C., Roehm, C., Lakshmanan, N., and Iyer, N. R. [2011] "Seismic retrofitting of nonductile beam-column sub-assemblage using FRP wrapping and steel plate jacketing," *Construction and Building Materials*, **25**(1), 175-182.

Sharma, A. [2013] "Seismic Behavior and Retrofitting of RC Frame Structures with Emphasis on Beam-Column Joints-Experiments and Numerical Modeling," PhD Dissertation, University of Stuttgart, Stuttgart.

Shafaei, J., Hosseini, A., and Marefat, M. S. [2014] "Seismic retrofit of external RC

beam-column joints by joint enlargement using prestressed steel angles," *Engineering Structures*, **81**, 265-288.

Sharbatdar, M. K., Kheyroddin, A., and Emami, E. [2012] "Cyclic performance of retrofitted reinforced concrete beam-column joints using steel prop," *Construction and Building Materials*, **36**, 287-294.

Sutcu, F., Takeuchi, T. and Matsui, R. [2014]. "Seismic retrofit design method for RC buildings using buckling-restrained braces and steel frames." *Journal of Constructional Steel Research*, 101, 304-313.

Uang, C. M. and Bertero, V. V. [1990]. "Evaluation of seismic energy in structures". *Earthquake Engineering & Structural Dynamics*, 19(1), 77-90.

Walker, S. G. [2001]. Seismic performance of existing reinforced concrete beam-column joints. M.S. thesis, University of Washington, Seattle, Washington.

Wong, H. F. and Kuang, J. S. [2008] "Effects of beam-column depth ratio on joint seismic behaviour," *Proceedings of the Institution of Civil Engineers-Structures and Buildings*, **161**(2), 91-101.

TABLE 1. Shear stress and strain of characteristic points for joint

Characteristic points	Exterior joint	Interior joint
Cracking strength(τ_c-γ_c)	τ_c= $0.48\sqrt{f_c}$, γ_c=0.00043[Jeon *et al.*, 2015]; $\tau_c \leq 0.6\tau_{max}$	
Yield strength(τ_y-γ_y)	τ_y=0.9τ_{max}, γ_y=0.005	
Peak strength(τ_{max}-γ_p)	$\tau_{max}=\sigma_1\sqrt{1+\frac{p_j}{\sigma_1}\frac{\cos\theta}{\cos(\pi/4)}}$, $\theta=\tan^{-1}(h_b/h_c)$ $\sigma_1=0.42\sqrt{f_c}$ [Priestley, 1997] (Reinforcement type of Fig. 1(b)); $\sigma_1=0.29\sqrt{f_c}$ [Priestley, 1997] (Reinforcement type of Fig. 1(c)) γ_p=0.015 [Jeon *et al.*, 2015]	$\sigma_1=0.84\sqrt{f_c}$ [Sharma, 2013] (Reinforcement type of Fig. 1(a)) γ_p=0.02 [Jeon *et al.*, 2015]
Residual strength(τ_r-γ_r)	τ_r=0.2τ_{max}, k_{deg}=-75 [Jeon *et*	τ_r=0.2τ_{max}, k_{deg}=-80 [Jeon *et*

al., 2015] *al.*, 2015]

Note: f_c is the concrete compressive strength (MPa); σ_1 is the maximum principal tensile stress (MPa); p_j is the joint average axial stress (MPa); h_b is the beam cross-sectional height; h_c is the column cross-sectional height; k_{deg} is the degradation gradient from peak strength point to residual strength point (MPa/rad); the shear strength of joint anchorage failure (Fig. 1(d)) was not discussed in this study.

FIGURE 1 Typical reinforcement details of non-seismically designed beam-column interior and exterior joints

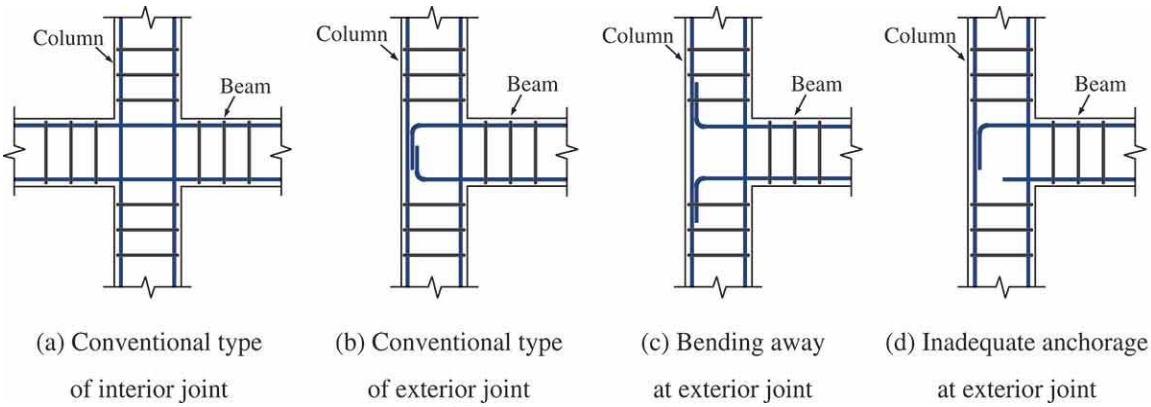

(a) Conventional type of interior joint

(b) Conventional type of exterior joint

(c) Bending away at exterior joint

(d) Inadequate anchorage at exterior joint

FIGURE 2 Design and test of the scaled BRH specimen

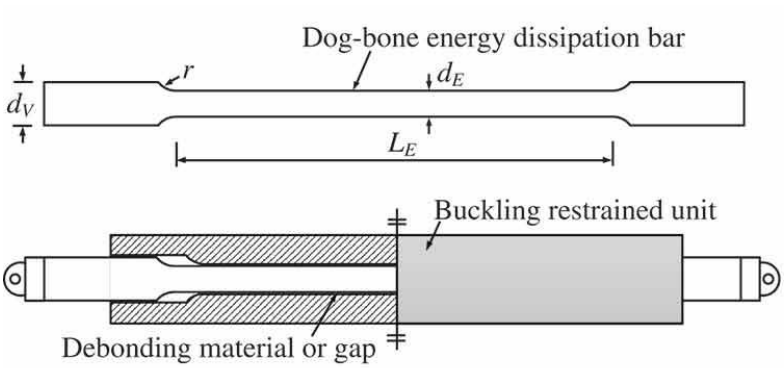

(a) Composition of typical BRH

(b) Assembled BRH

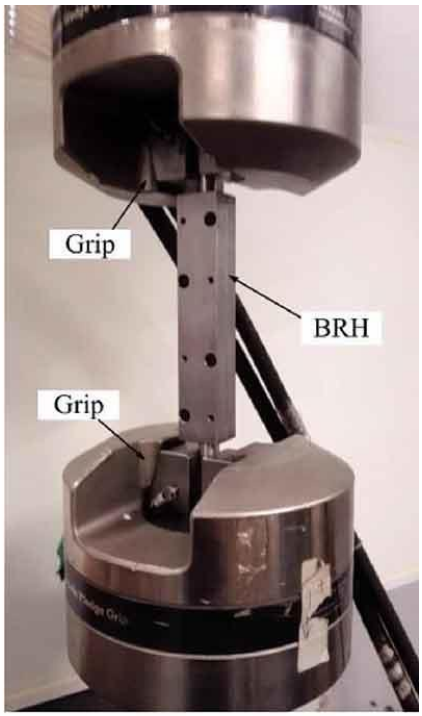

(c) View of scaled BRH specimen under test

FIGURE 3 Comparison between experimental result and numerical simulation of BRH behaviour

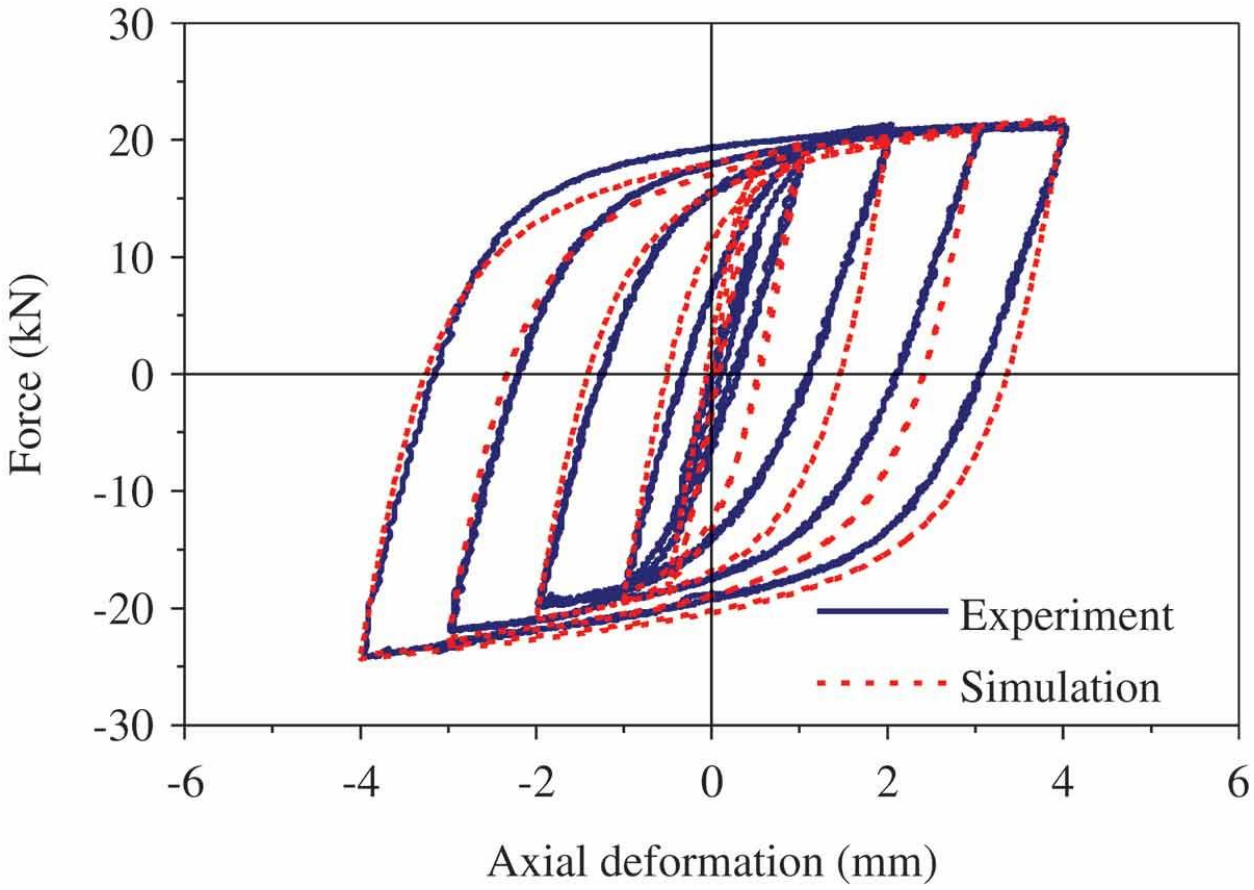

FIGURE 4 Typical failure modes for non-seismically designed beam-column joint

(a) Joint shear failure

[Au *et al*., 2005]

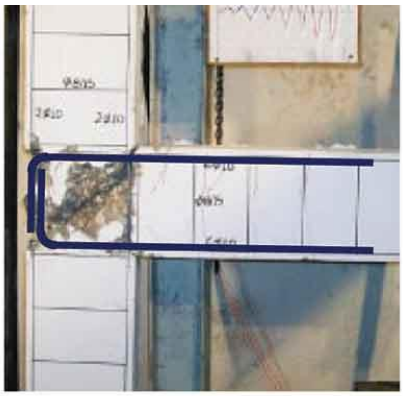

(b) Joint shear failure

[Karayannis *et al*., 2008]

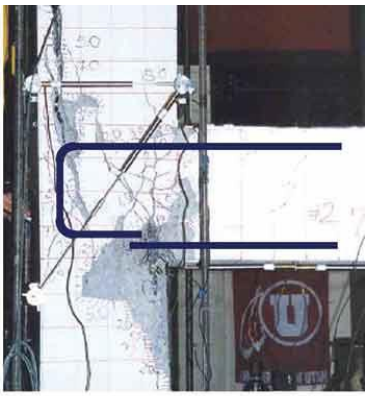

(c) Anchorage failure

[Pantelides et al., 2002]

FIGURE 5 Numerical model of beam-column joint assemblage

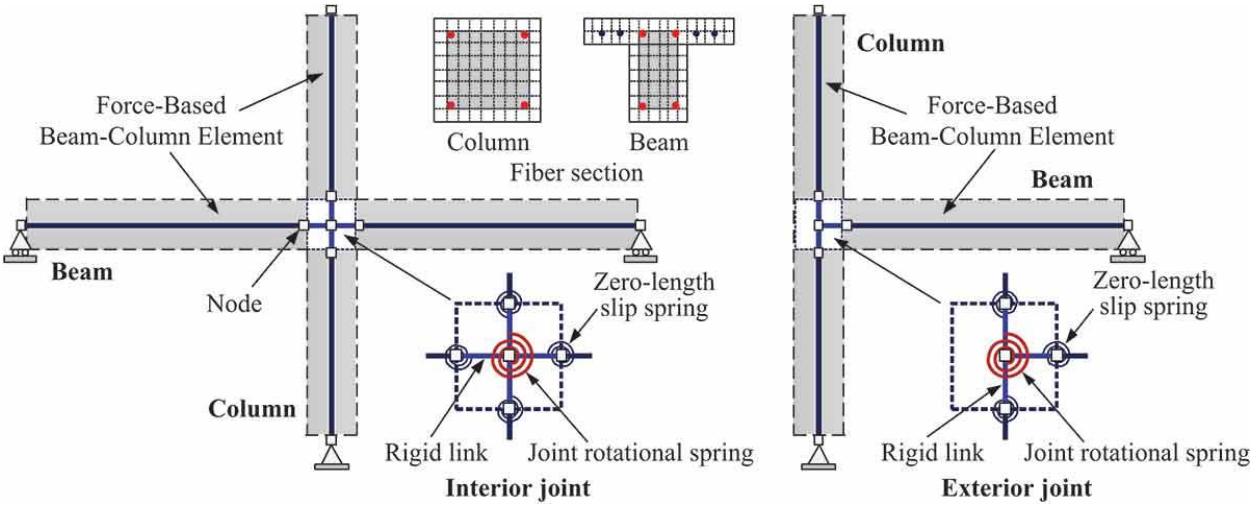

FIGURE 6 Bar-slip deformation in beam–column joint

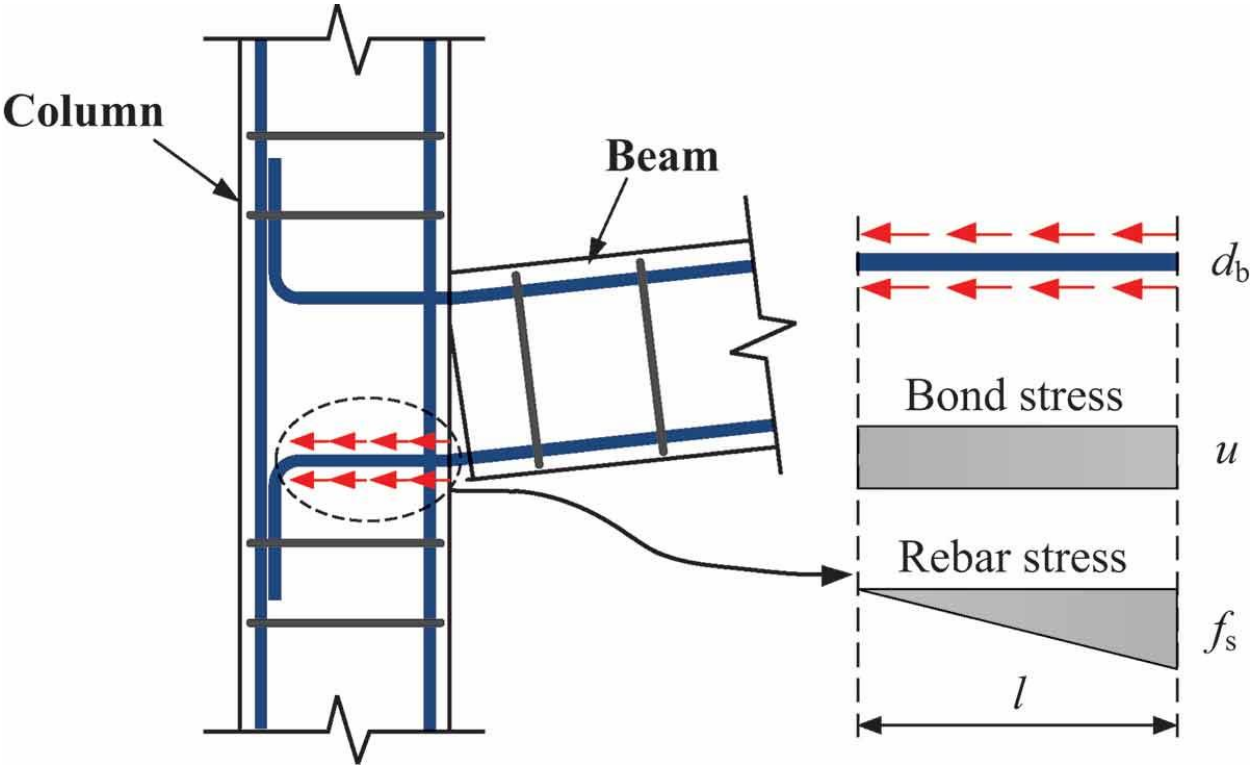

FIGURE 7 Constitutive model for Pinching4 material

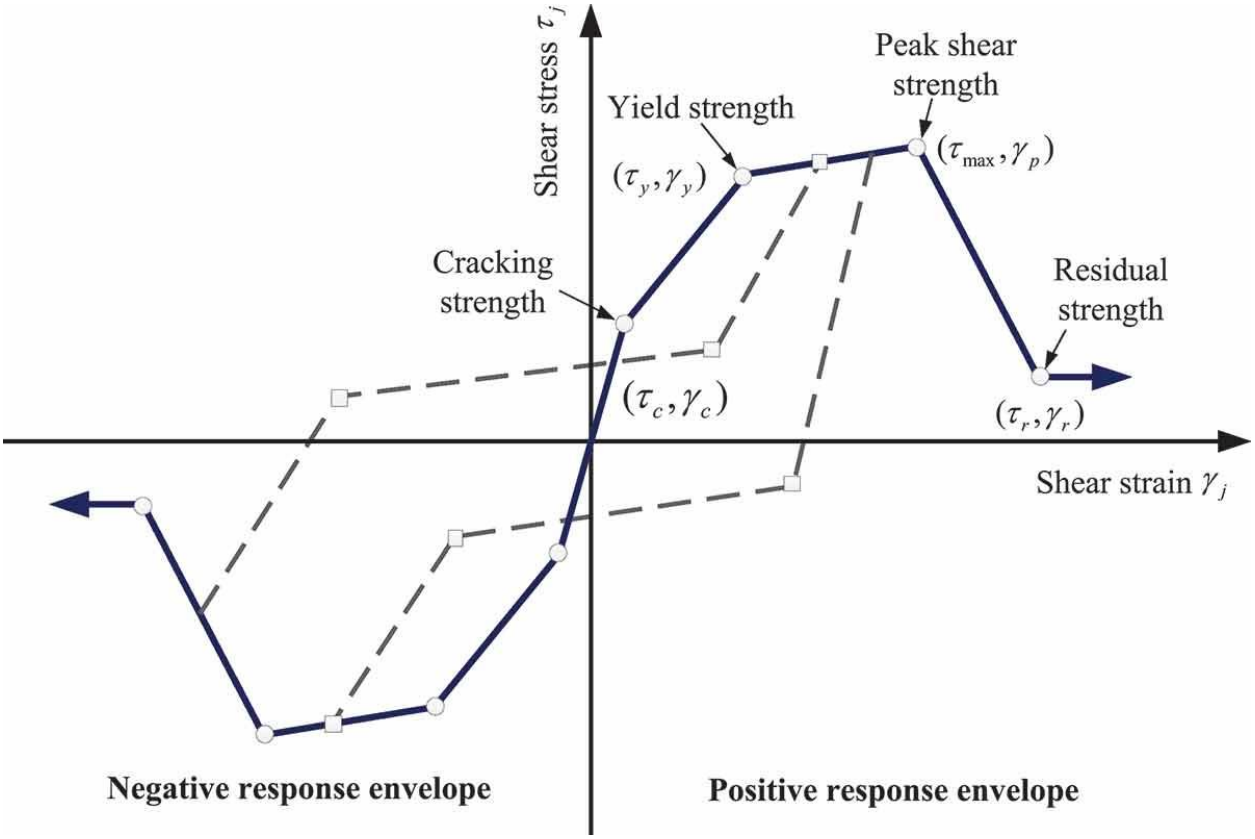

FIGURE 8 Comparison of the force-displacement relationships between the experimental and numerical results of non-seismic RC joints

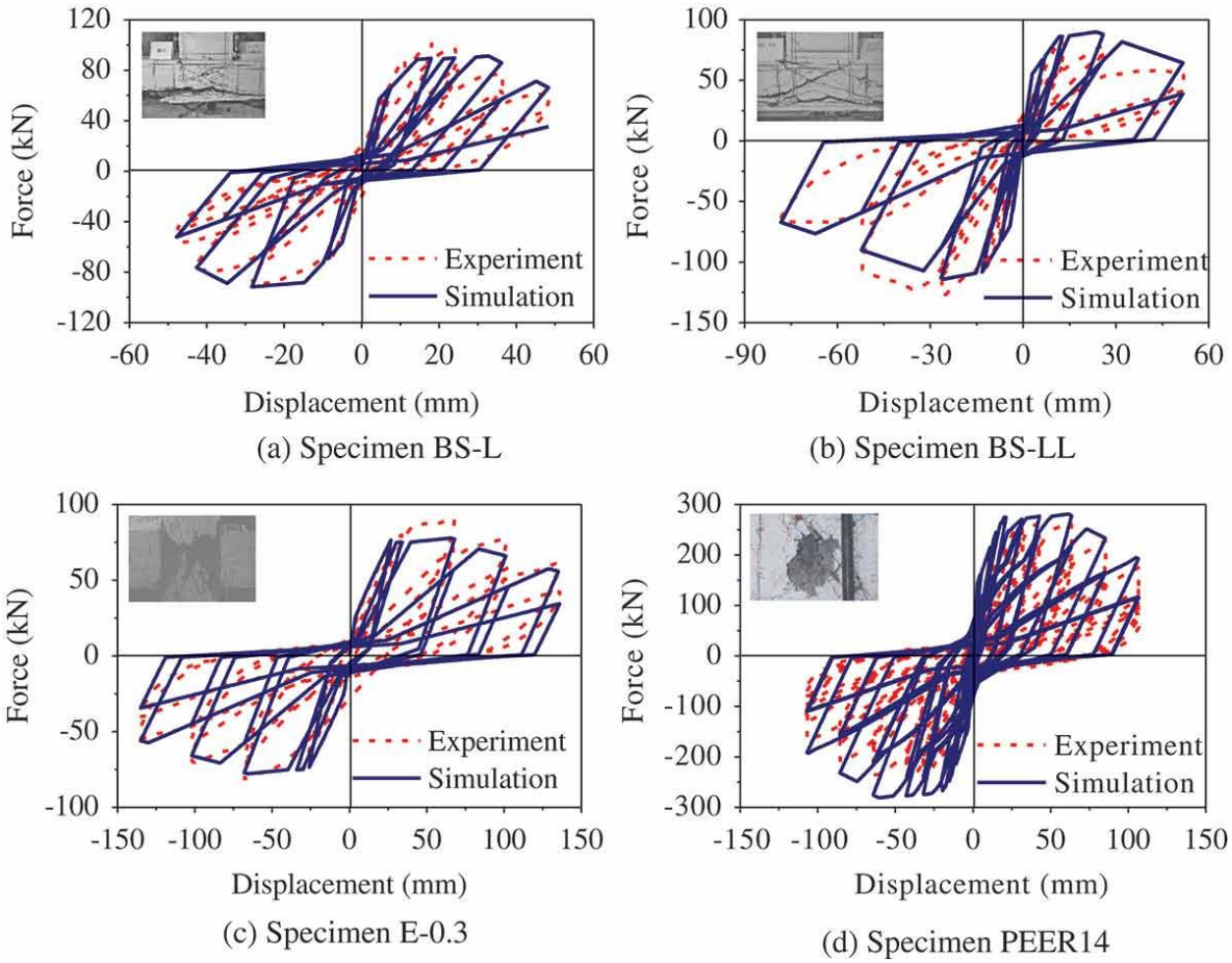

FIGURE 9 Retrofit solutions for interior and exterior joint with BRHs

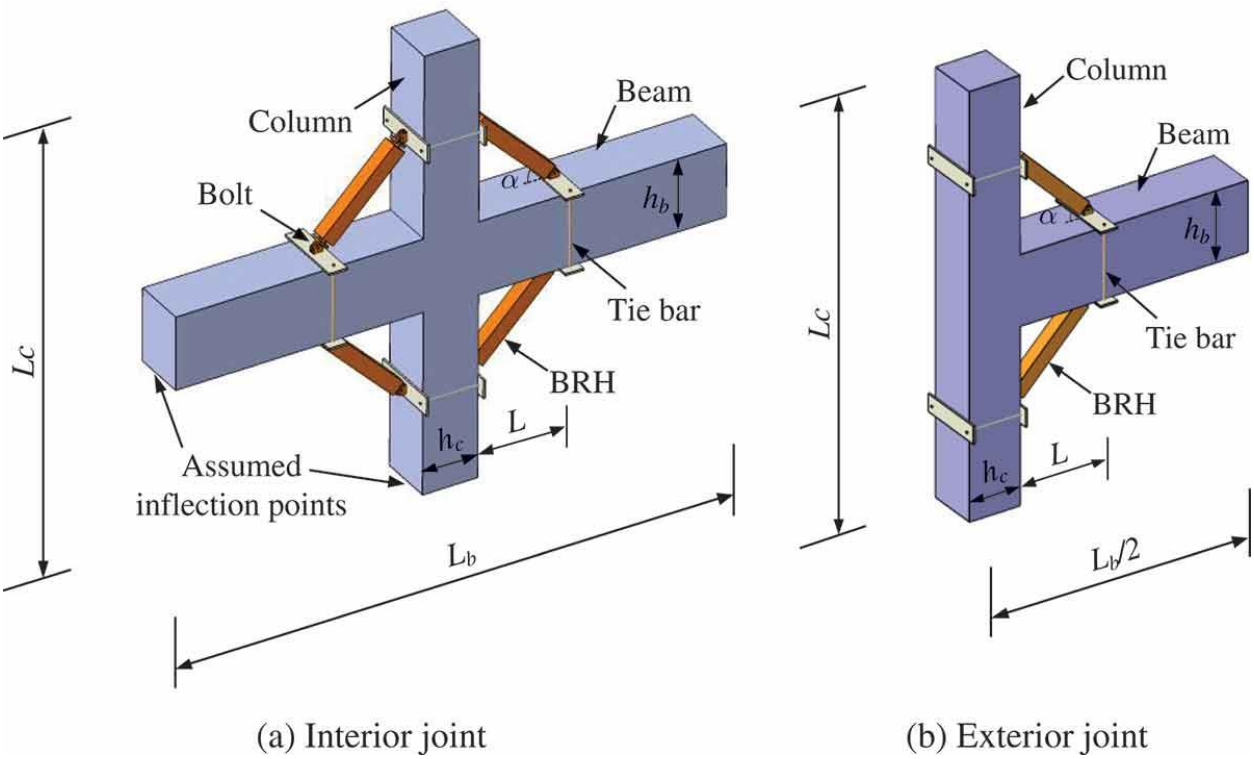

FIGURE 10 Internal force distribution for retrofitted exterior joint with BRHs

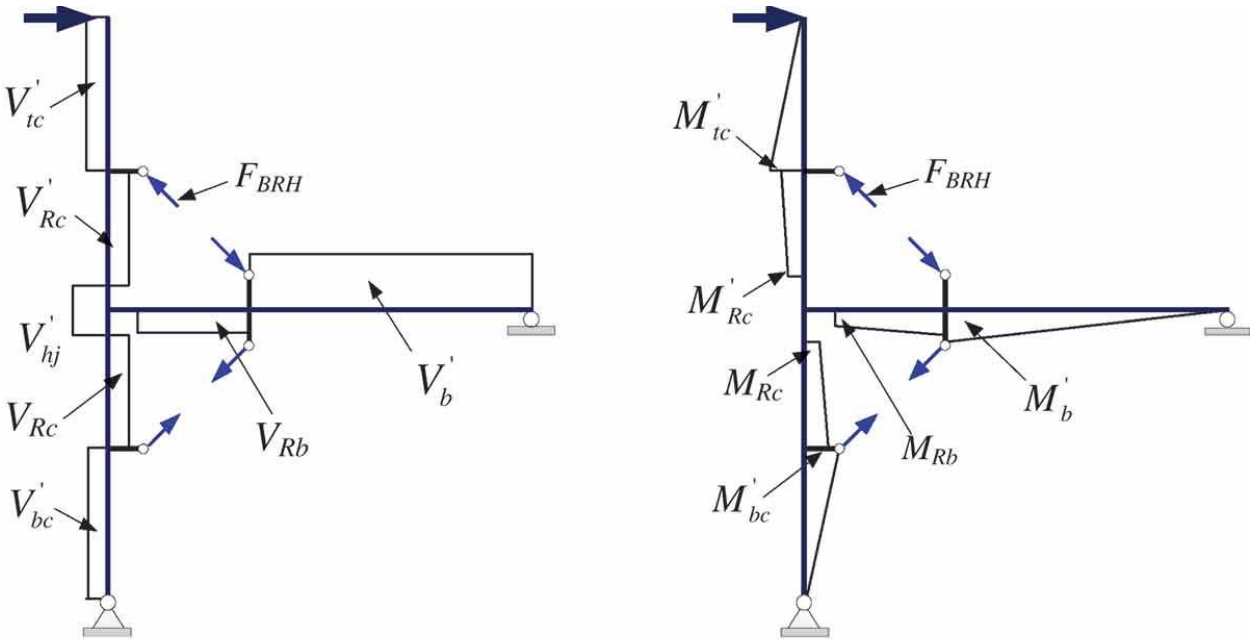

(a) Shear force distribution

(b) Moment distribution

FIGURE 11 Flowchart of the retrofit design procedures for RC joint with BRHs

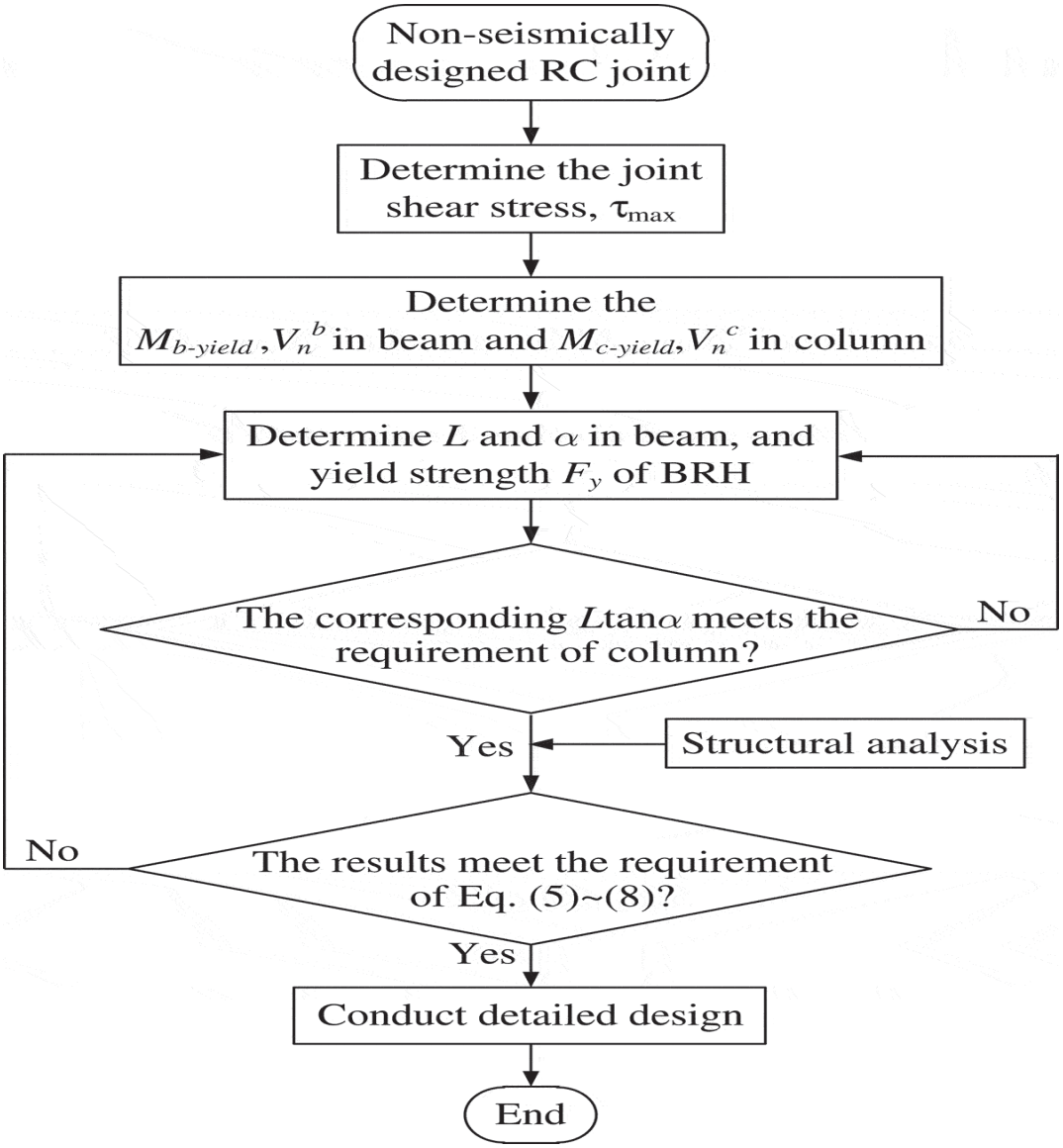

FIGURE 12 Geometric properties and reinforcement details of joint specimens

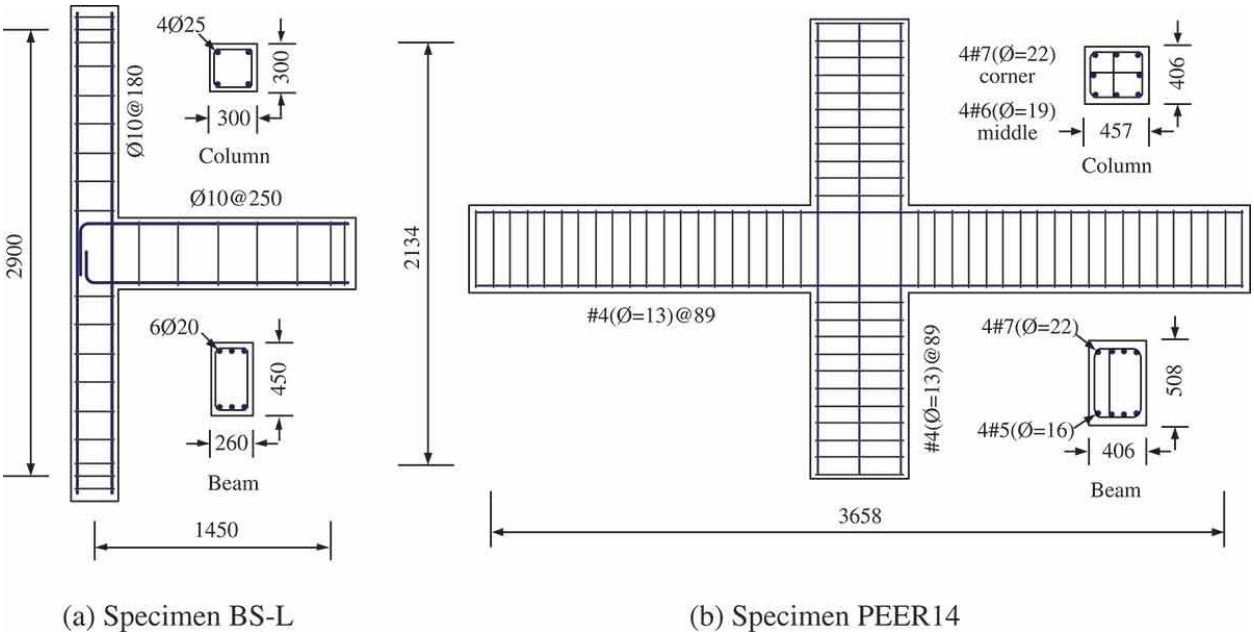

(a) Specimen BS-L (b) Specimen PEER14

FIGURE 13 Loading protocols for test and numerical analysis

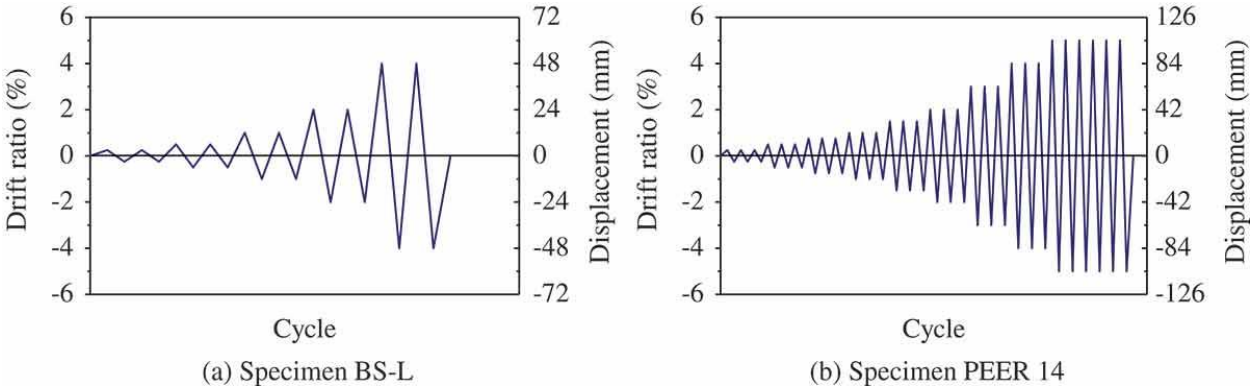

FIGURE 14 Force-displacement hysteretic relationships of the retrofitted specimens

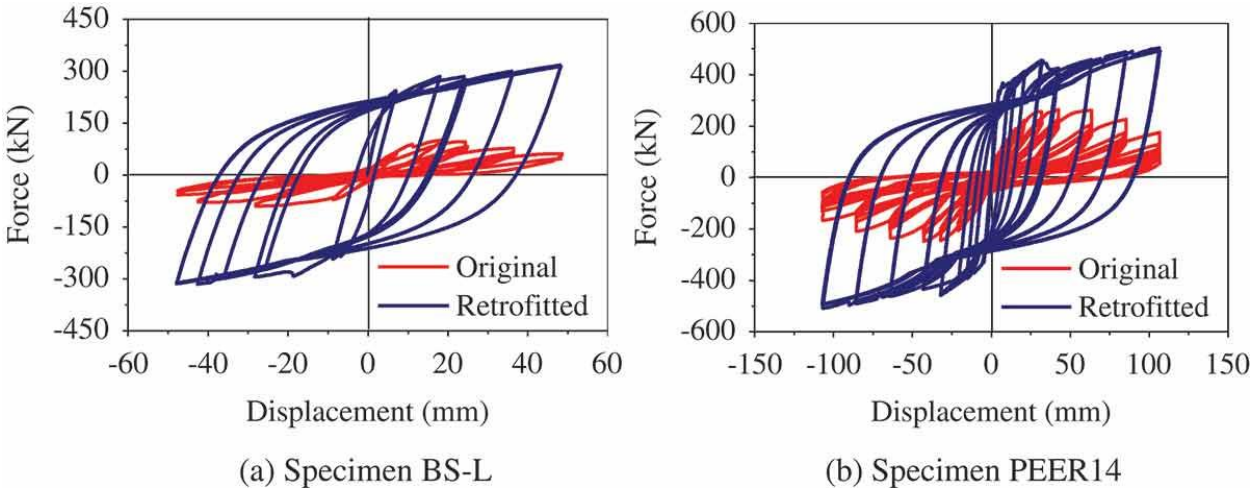

FIGURE 15 Joint shear stress versus strain response for specimen BS-L

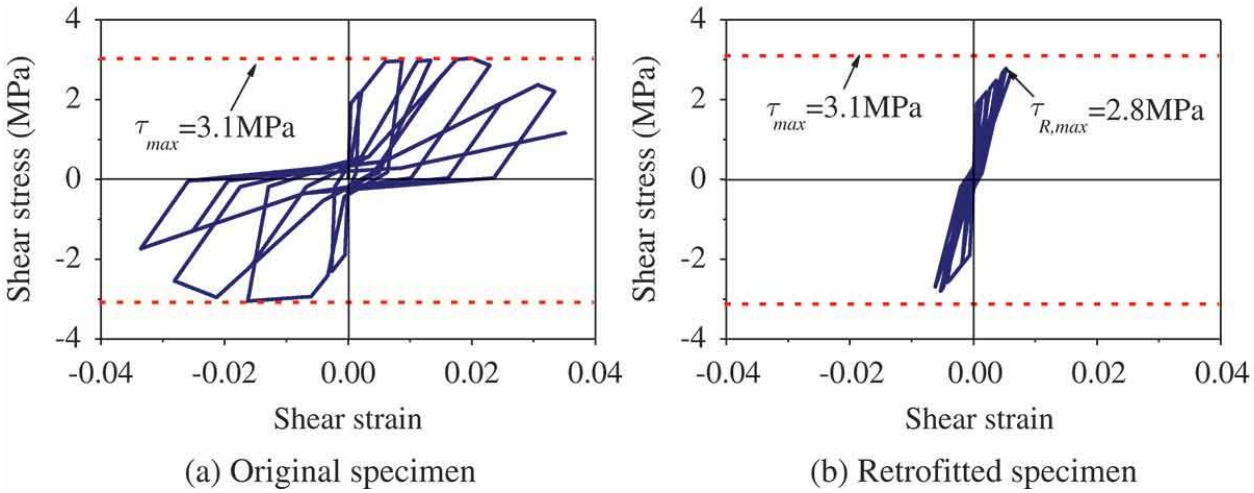

FIGURE 16 Joint shear stress versus strain response for specimen PEER14

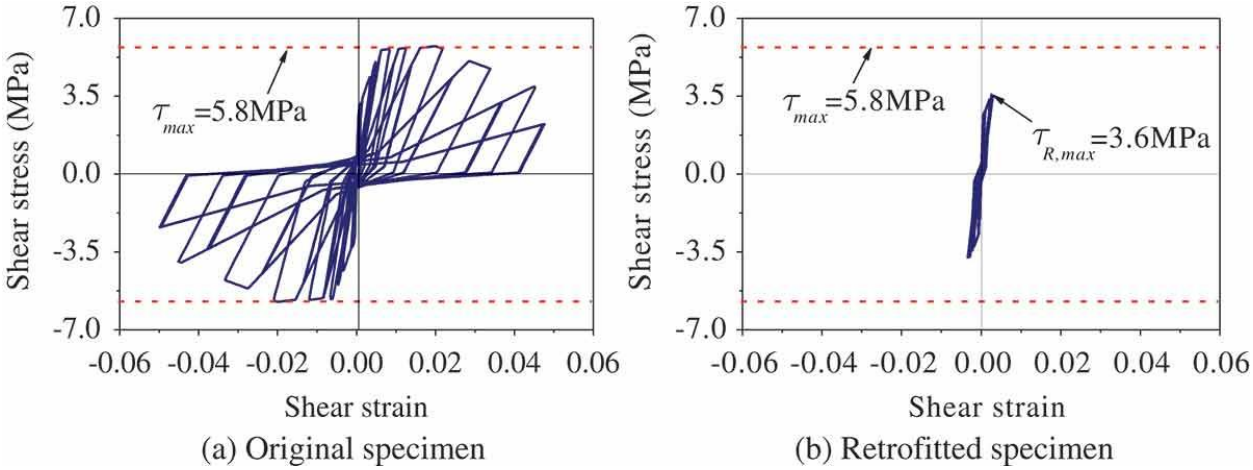

FIGURE 17 Damage modes of the retrofitted joints with BRHs

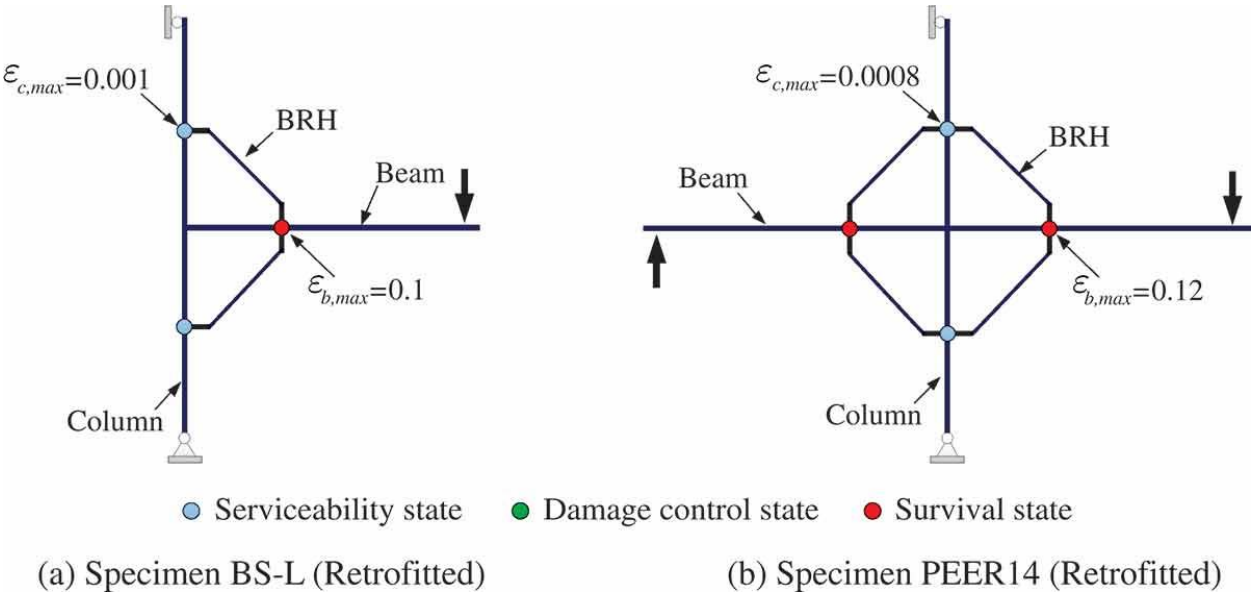

(a) Specimen BS-L (Retrofitted) (b) Specimen PEER14 (Retrofitted)

FIGURE 18 Force-displacement hysteretic relationships of BRHs

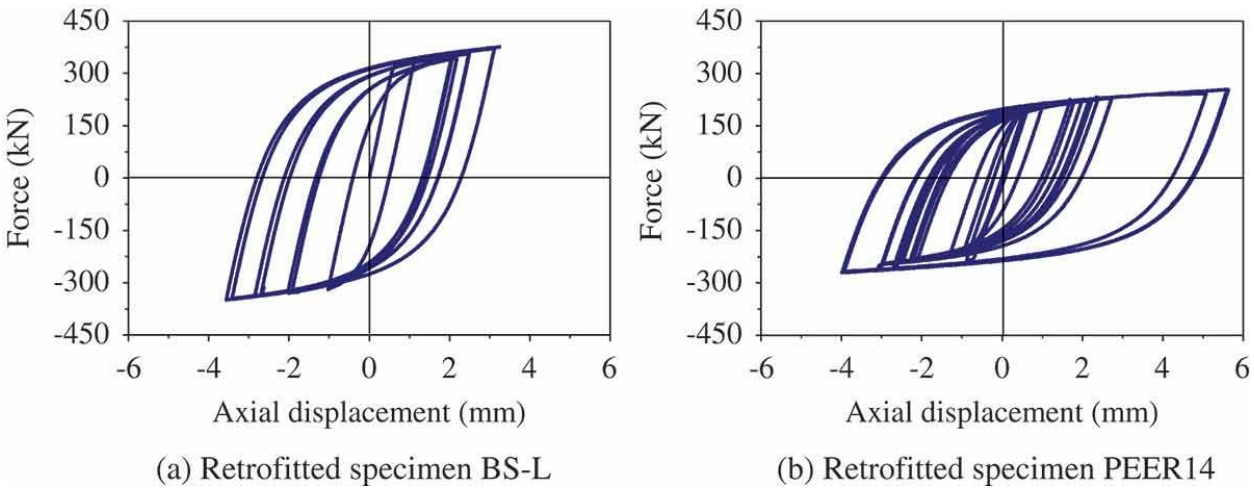

FIGURE 19 Comparison of cumulative energy dissipation in the whole cyclic loading